FRONTIERS OF PHYSICS

LETTER
Volume 19 / Issue 6 / 63209 / 2024

Interlayer ferromagnetic coupling in nonmagnetic elements doped CrI_3 thin films

Xuqi Li[1,*], Xuyan Chen[2,*], Shiyang Sun[1,*], Huihui Zhang[1], Haidan Sang[1], Xiaonan Wang[3], Shifei Qi[1,4,†], Zhenhua Qiao[4,‡]

1 College of Physics and Hebei Advanced Thin Film Laboratory, Hebei Normal University, Shijiazhuang 050024, China
2 School of Gifted Young, University of Science and Technology of China, Hefei 230026, China
3 School of Chemistry and Materials Science, Hebei Normal University, Shijiazhuang 050024, China
4 International Center for Quantum Design of Functional Materials, CAS Key Laboratory of Strongly-Coupled Quantum Matter Physics, and Department of Physics, University of Science and Technology of China, Hefei 230026, China
*These authors contributed equally to this work.
Corresponding authors. E-mail: †qisf@hebtu.edu.cn, ‡qiao@ustc.edu.cn
Received October 2, 2023; accepted April 6, 2024

ABSTRACT

The exploration of magnetism in two-dimensional layered materials has attracted extensive research interest. For the monoclinic phase CrI_3 with interlayer antiferromagnetism, finding a static and robust way of realizing the intrinsic interlayer ferromagnetic coupling is desirable. In this work, we study the electronic structure and magnetic properties of the nonmagnetic element (e.g., O, S, Se, N, P, As, and C) doped bi- and triple-layer CrI_3 systems via first-principles calculations. Our results demonstrate that O, P, S, As, and Se doped CrI_3 bilayer can realize interlayer ferromagnetism. Further analysis shows that the interlayer ferromagnetic coupling in the doped few-layer CrI_3 is closely related to the formation of localized spin-polarized state around the doped elements. Further study presents that, for As-doped tri-layer CrI_3, it can realize interlayer ferromagnetic coupling. This work proves that nonmagnetic element doping can realize the interlayer ferromagnetically-coupled few-layer CrI_3 while maintaining its semiconducting characteristics without introducing additional carriers.

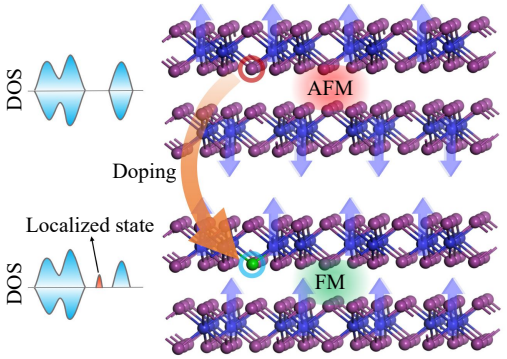

Keywords ferromagnetism, magnetic doping

1 Introduction

Two-dimensional (2D) magnetic semiconductors have attracted extensive attention due to the enormous potential for novel magneto-optic [1–6], magnetoelectronic [7–14], and spintronic devices [15–17]. As a representative 2D layered material, CrI_3 possesses its own unique physical properties. The bulk CrI_3 has two different structures, i.e., high-temperature monoclinic phase and low-temperature rhombohedral phase. The bilayer CrI_3 with rhombohedral stacking exhibits interlayer ferromagnetic coupling, while that with monoclinic stacking exhibits interlayer antiferromagnetic coupling [18–25], and their phase transition temperature is 220 K [26]. Thus, the magnetic order of CrI_3 is susceptible to the variation of layer thickness and stacking order. Previous first-principles calculations have predicted that interlayer magnetic coupling can be effectively modulated by stacking order in bilayer [18, 20, 21]. Later experiments [23, 24] proved that different stacking orders can affect the observed

Higher Education Press

https://doi.org/10.1007/s11467-024-1435-2

magnetic states of CrI_3 in both bulk and few-layer CrI_3 systems.

In van de Waals layered systems, the relatively weak interlayer coupling indicates that the interlayer magnetic order can be easily tuned via external means. Indeed, it was experimentally reported that monoclinic bilayer CrI_3 can be transformed from interlayer antiferromagnetic to ferromagnetic coupling by applying electric gating [13, 27–29]. A possible physical mechanism describing this magnetic transition is the formation of magnetic polaron, which was theoretically confirmed [30]. Beside above external electric gating, a natural question arises: whether it is possible to find a static and robust way of realizing the intrinsic interlayer ferromagnetic coupling in few-layer CrI_3? In addition, for semiconductor materials, the carrier doping concentration may destroy the physical properties. Therefore, it is desirable to realize the interlayer ferromagnetically-coupled few-layer CrI_3 while maintaining its semiconducting characteristics without introducing additional carriers.

In this study, we perform a systematic study on the magnetic and electronic properties of nonmagnetic-element doped few-layer CrI_3 by using first-principles calculation methods. We first show that the interlayer ferromagnetic coupling can be established in bilayer CrI_3 doped with C, N, O, P, S, As, or Se. We then find that the interlayer ferromagnetic coupling is intimately related to the formation of localized spin-polarized state around the doped nonmagnetic elements. Especially for the As-doped bi- or tri-layer CrI_3, it can realize interlayer ferromagnetism and does not introduce extra carriers, therefore maintaining the system's semiconducting properties.

2 Calculation methods

Our first-principle calculations were performed by using the projected augmented-wave method [31] as implemented in the Vienna ab initio simulation package (VASP) [32, 33]. The generalized gradient approximation (GGA) of Perdew–Burke–Ernzerhof (PBE) type was used to treat the exchange-correlation interaction [34]. In our calculations, the lattice constant of the high-temperature phase of CrI_3 was chosen to be $a_0 = 6.92$ Å [20]. A vacuum buffer space of 15 Å was used to prevent the coupling between adjacent slabs. The kinetic energy cutoff was set to be 340 eV. With fixed supercells, all structures were fully relaxed. The van der Waals (vdW) force was taken into account by employing the Grimme's method (DFT-D2) [35]. The Brillouin-zone integration was carried out by using $5 \times 5 \times 1$ Monkhorst–Pack grids. Unless mentioned otherwise, GGA+U [36, 37] method was used with the on-site repulsion parameter $U = 3.9$ eV and the exchange parameter $J = 1.1$ eV [20], where U is for the more localized $3d$ orbitals of Cr atoms. Additionally, conventional DFT may fail to predict the charge localization due to inherent self-interaction error, even if DFT+U method has been employed [38]. The self-interaction effects can be effectively canceled by the HF/DFT hybrid approach, which has successfully predicted electronic structures in many semiconductors [39]. We employed a PBE-based Heyd–Scuseria–Ernzerhof functional in which 75% of the PBE exchange is combined with 25% of the nonlocal Hartree–Fock exchange, and the screening parameter that separates the exchange potential [40] into short-range and long-range parts was set at 0.2.

3 Experimental possibility of element doping

We first study the possibility of element doping in bilayer CrI_3, i.e., substituting I by nonmagnetic dopants. Some typical candidates of nonmagnetic dopants including O, S, Se, N, P, As, and C are considered. As displayed in Fig. 1(a), there are two types of I-doping sites labelled as I_1 (at the surface) and I_2 (inside the interlayer). The formation energy was obtained by using the expression [41–43] $\Delta H_F = E^D_{tot} - E_{tot} - \Sigma n_i \mu_i$, where E^D_{tot} is the total energy of the system including one nonmagnetic impurity, E_{tot} is the total energy of the system, μ_i is the chemical potential for the species i (host atoms or dopants), and n_i is the corresponding number that was added/removed from the system.

As displayed in Fig. 1(b), for O, S, Se, N substitutions at two I sites in the same CrI_3 layer, the formation energy is within the range of –0.4 to 1.5 eV. It indicates that the I_1 substitutional site is preferred due to smaller formation energy than that at I_2 substitution. For example, N substitution leads to smaller formation energy (about –0.6 to 0.2 eV) than those from O (about –0.2 to 0.2 eV), S (about 0.4 to 0.9 eV) and Se (about 1.1 to 1.4 eV) substitution in the whole range of the accessible host element chemical potentials. However, for P, As, and C substitutions [see Fig. 1(c)], they have larger formation energies than those with O, S, Se, or N dopants. In addition, we find that the I_1 substitutional site is preferred by P and C, while I_2 substitutional site is preferred by As. The formation energy shows that all candidate elements (except As) are more stable at I_1 position. The formation energy of As substituted I_2 site is positive (about 2.3 to 2.7 eV). It is noteworthy that C-doped ZnO has been experimentally fabricated even the estimated formation energy is about 5.3 eV [44], which is much larger than all element-doped CrI_3. Therefore, it is reasonable to believe that O, S, Se, N, P, and As doped CrI_3 bilayer could be experimentally fabricated. In fact, we also performed the test calculations of different doped configurations including possible interstitial sites

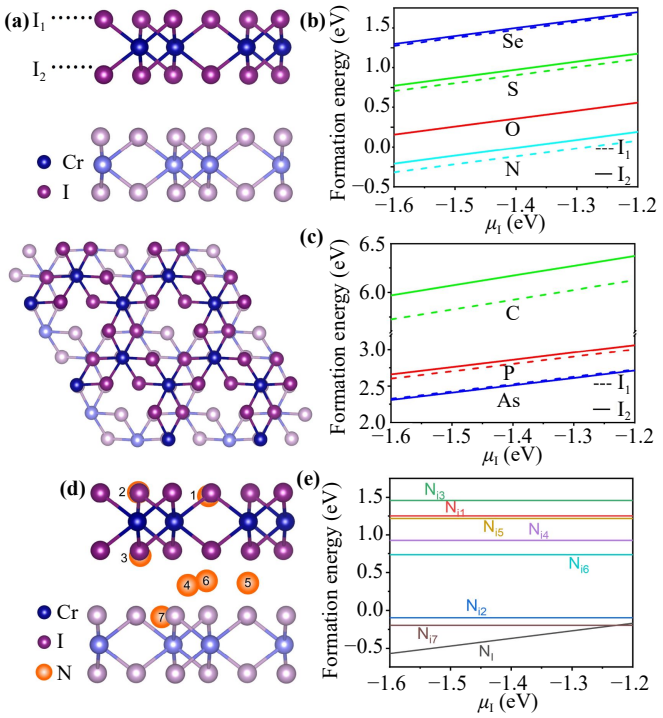

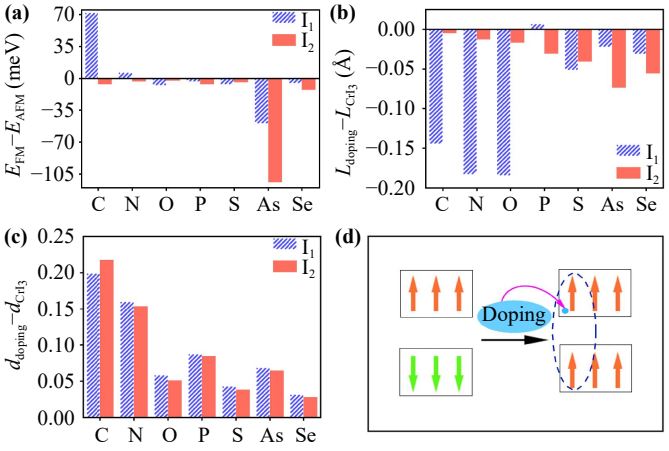

Fig. 1 **(a)** Side and top views of crystal structures of high-temperature monoclinic bilayer CrI_3 phase and the substitution sites are labeled as I_1 and I_2. Formation energies of **(b)** O, S, Se, N and **(c)** P, As, or C element-doped bilayer CrI_3 as a function of the host element chemical potentials. Possible interstitial sites **(d)** and the formation energy **(e)** as a function of chemical potential for interstitial and substitutional configurations in the N doped bilayer CrI_3.

Fig. 2 **(a)** Energy difference between interlayer ferromagnetic (FM) and antiferromagnetic (AFM) states. **(b)** Difference of interlayer distance between doping configuration and pristine CrI_3. **(c)** Charge difference between Cr atoms near doping site in the doped and pristine bilayer CrI_3. **(d)** Schematic illustration of localized spin-polarized state-mediated interlayer ferromagneitic coupling in doped bilayer CrI_3.

in the N doped bilayer CrI_3. Formation energies for both substitution and interstitial configurations are shown in Figs. 1(d) and (e). We can find that the N substitutional site is still preferred. In our study, all doping sites are nonmetal substitutions similar to N doping. Similar doping character might exist in this study. Hence, we mainly focus on the anion substitutional doping.

4 Magnetic properties

We now move to investigate the interlayer magnetic coupling of the doped CrI_3. Figure 2(a) displays the energy difference $\Delta E = E_{FM} - E_{AFM}$ between interlayer ferromagnetic and antiferromagnetic states for different element-doped bilayer CrI_3. As reported, the pristine bilayer CrI_3 exhibits interlayer antiferromagnetic coupling [18, 20, 21]. The introduction of dopants except C and N leads to $\Delta E < 0$, indicating the formation of interlayer ferromagnetism. For the O, P, S, As, and Se substitution at $I_1(I_2)$ site [see Fig. 2(a)], ΔE are respectively –7.7(–2.2), –3.6(–6.3), –6.7(–4.0), –49.7(–113.9), and –5.4(–12.3) meV, indicating the interlayer ferromagnetic coupling. As a contrast, it maintains the interlayer antiferromagnetism in C or N doped case. We also estimated the Curie temperature for the O, P, S, Se, and As doped bilayer CrI_3 using the mean-field approximation. For the As doped bilayer CrI_3, the estimated Curie temperature is about 18.35 K. In addition, the test calculations of energy difference between interlayer FM and AFM configurations of As doped bilayer CrI_3 using different vdW corrections were also performed. From our calculations, the different vdW corrections except DFT-ulg provide a qualitative agreement conclusion that interlayer FM coupling can appear in As doped bilayer CrI_3. However, an obvious difference related to strong (DFT-D2 [35] and DFT-D3 [45]) or weak (vdW-DF [46], vdW-DF2 [47], optB86b-vdW [48], optB88-vdW [49], optPBE-vdW [49]) interlayer FM coupling exists. It is also noted that DFT-D2 correction used in this study indeed gives correct predictions of interlayer AFM coupling in bilayer CrI_3 (energy difference between FM and AFM configuration is about 8.78 meV) and interlayer FM coupling in trilayer CrI_3 (FM configuration is the most stable one among of four magnetic configuration, as listed in Table 1), which are in agreement with experimental observations [1]. Hereinbelow, we choose the I_2-site As-doped bilayer CrI_3 as an example to analyze the origin of the interlayer ferromagnetism.

For vdW magnetic materials, many studies have shown that the interlayer distance plays a crucial role in determining the interlayer magnetic coupling [50–53]. Thus, we first investigate the relationship between the interlayer distance and the energy difference ΔE. Figure 2(b) displays the difference of interlayer distances between doped and pristine CrI_3. One can find that the interlayer distances in nearly all doped systems (except

Table 1 The structural and magnetic properties of As doped trilayer CrI_3. The spin direction of each layer is denoted by the up/down arrow. The ground state of each dopant is denoted by red. The energy differences between the specific structure and ground state are shown. The energy is in unit of meV.

Structure	$\Delta_E(\uparrow\downarrow\uparrow)$	$\Delta_E(\uparrow\uparrow\downarrow)$	$\Delta_E(\uparrow\downarrow\downarrow)$	$\Delta_E(\uparrow\uparrow\uparrow)$
CrI_3	1.99	4.55	12.89	0
As_1	15.15	119.91	121.58	11.52
As_2	37.22	127.3	147.85	20.44
As_3	78.56	100.28	85.28	0

P-doped configuration at I_1 substitution) decrease with respect to the pristine case. Particularly, the interlayer distances in C, N, and O doped systems at I_1-site substitution shrink respectively about 0.14, 0.17, and 0.18 Å, which are much larger than that in the As-doped system. These together show that there is no obvious correlation between the strength of ferromagnetic coupling and the interlayer distance.

It was reported that the interlayer magnetism of vdW materials is closely related to different 3d electron occupation between different layers [54–56]. In Fig. 2(c), we display the charge difference of Cr atoms near the dopants between the doped and pristine bilayer CrI_3. It shows that the charge of Cr atoms near dopants increases for all doped systems. However, in As-doped bilayer, the change of 3d electron occupation due to doping is much less than those of the C and N doped bilayers. Therefore, the difference of $3d$ electrons occupation between two layers cannot explain the formation of the interlayer ferromagnetism. For the C and N doped bilayer CrI_3, interlayer AFM coupling is still reserved. From our calculations the bound magnetic polaron does not appear due to more electrons from the doping are delocalized. And therefore, no magnetic transition from interlayer AFM coupling to FM coupling appear in the C and N doped bilayer CrI_3.

We now move to calculate the differential charge densities of pristine and As-doped systems [see Figs. 3(a) and (b)] [20, 57]. One can see that As-doping indeed leads to obvious change of charge distribution inside the interlayer space. Figures 3(c) and (d) display the spin densities of pristine and doped cases, respectively. For pristine case, it exhibits intralayer ferromagnetism and interlayer anti-ferromagnetism. After As-doping, the interlayer anti-ferromagnetism transits to ferromagnetism, accompanying with a strongly localized spin-polarized state near the doping site. To confirm this finding, we have performed HSE06 calculations of all elements doped CrI_3 systems. For the As doped CrI_3, as presented in the Figs. 3(e) and (f), the electronic structures from PBE+U and HSE06 are qualitative agreement. Importantly, a sharp local density of state also appears in the band gap of the As doped CrI_3 from the HSE06

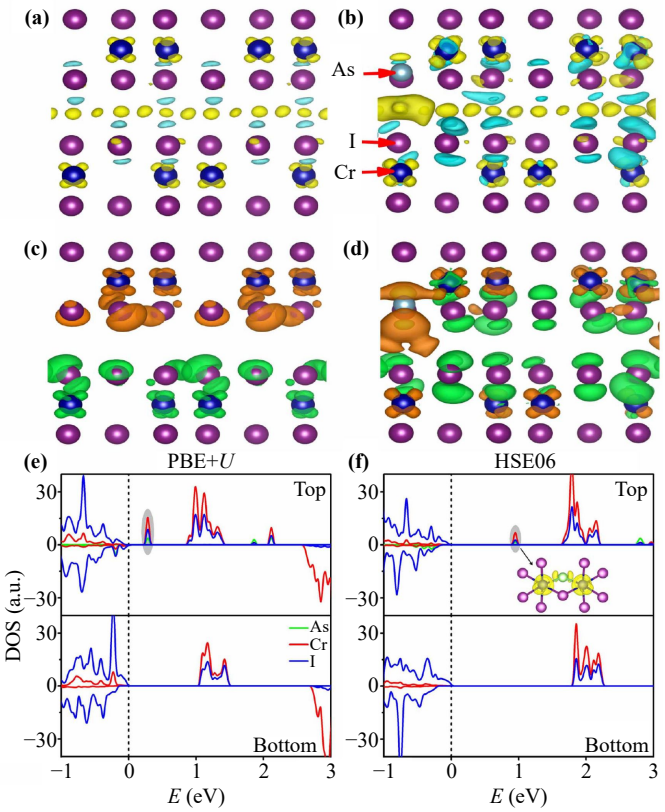

Fig. 3 Differential charge density of **(a)** pristine and **(b)** As-doped bilayer CrI_3. Spin density of **(c)** pristine and **(d)** As-doped bilayer CrI_3. Local density of states from **(e)** PBE+U and **(f)** HSE06 calculations in As-doped bilayer CrI_3. Yellow and blue isosurfaces represent respectively charge accumulation and reduction. Red and green isosurfaces represent respectively spin up and spin down. Cr-d, I-p and As-p orbitals in each layer of CrI_3 are displayed. In addition, band-decomposed charge density of the localized electron state is shown in the inset of (f).

calculation. By the band-decomposed charge density of the localized electron state in Fig. 3(f), we can find that it is evidently that excess electron is trapped around the doped As atom and a local lattice distortion appears accompanied by electron trapping. It is worth noting that this localized state is not self-trapped and it is related to doped defects similar to bound magnetic polaron suggested in diluted magnetic semiconductors [58] and 2D magnetic semiconductor [59].

To further confirm this physical origin, in Fig. 4, we display the density of states of the O, P, S, and Se doped bilayers, where O, P, S, and Se doped systems exhibit interlayer ferromagnetism. While for these doped systems, spin-polarized bound states arise based on PBE+U and HSE06 calculations. These suggest a direct evidence that the interlayer ferromagnetic coupling in doped bilayer CrI_3 is a consequence of the formation of localized spin-polarized state.

Another striking transport phenomenon is the insulating

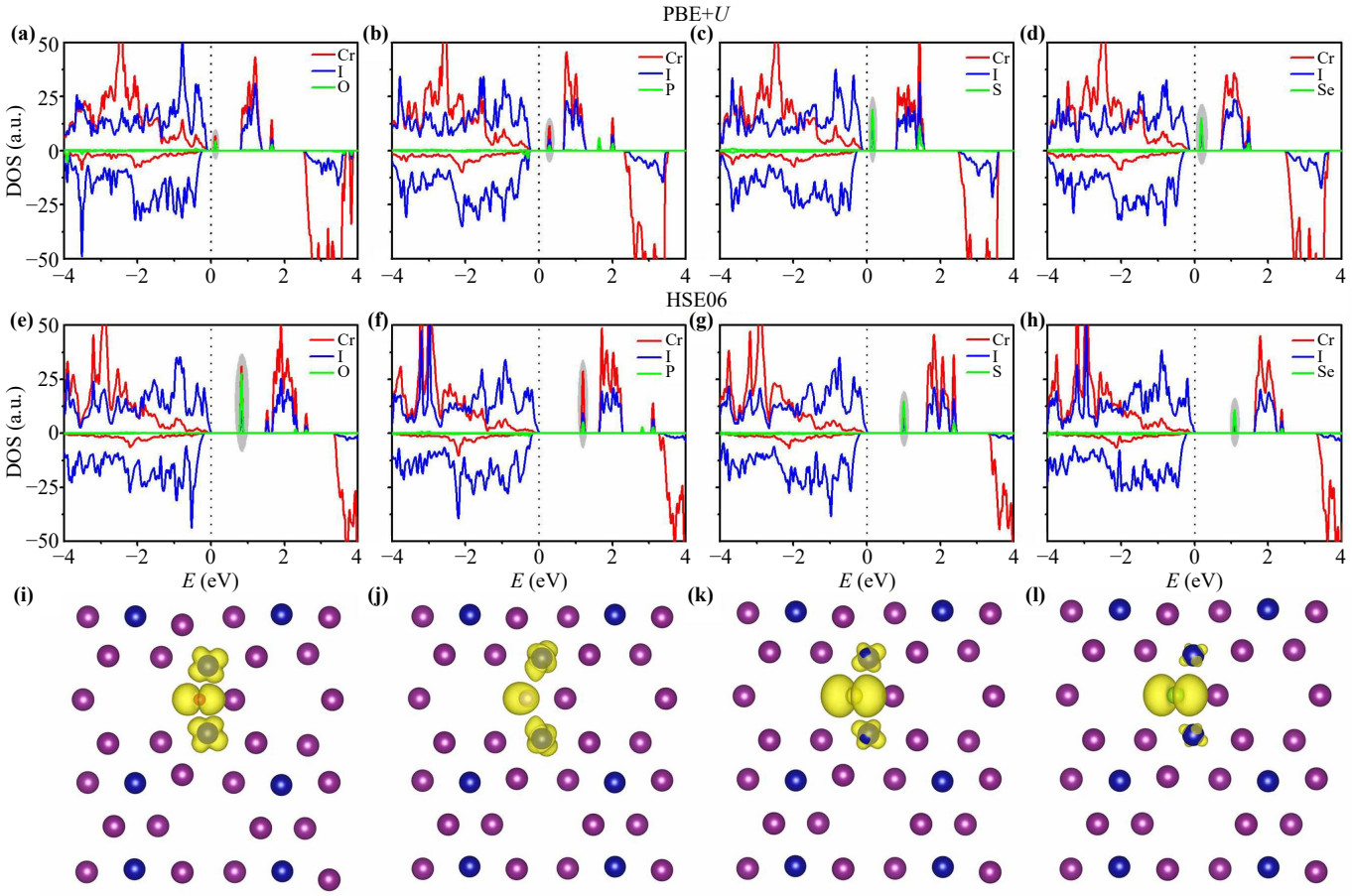

Fig. 4 The density of states in ferromagnetic state of **(a)** O, **(b)** P, **(c)** S, and **(d)** Se doped CrI_3 bilayer from PBE+U calculations. The density of states in ferromagnetic state of **(e)** O, **(f)** P, **(g)** S, and **(h)** Se doped CrI_3 bilayer from HSE06 calculations. Band-decomposed charge density of the localized electron state in ferromagnetic state of **(i)** O, **(j)** P, **(k)** S, and **(l)** Se doped CrI_3 bilayer from HSE06 calculations. The shadow part indicates the formation of spin-polarized state.

nature after doping. It is known that doping or gating can result in the ferromagnetism of semiconductors, but may also break the semiconducting property due to the carrier injection. Surprisingly, for O, P, S, As, and Se doped bilayer CrI_3, our results show that they exhibit both ferromagnetic and insulating features. In association with the experimental finding that different gate doping levels do not lead to n- or p-type conduction of bilayer CrI_3 dominantly with affected magnetic properties [13], it is believed that only insulated interlayer ferromagnetism in few-layer CrI_3 can be observed due to the formation of spin-polarized bound state at certain doping concentrations.

So far, we have shown that element doping in bilayer CrI_3 can induce interlayer ferromagnetism. The trilayer CrI_3 has weak interlayer ferromagnetic coupling [1]. Whether the element doping can enhance the interlayer ferromagnetism? By taking As-doping as an example in Fig. 5(a), three I substituted sites including I_1, I_2, and I_3 are selected. The interlayer magnetic couplings and their relative stabilities are respectively displayed in Fig. 5(b) and Table 1. One can see that the state with

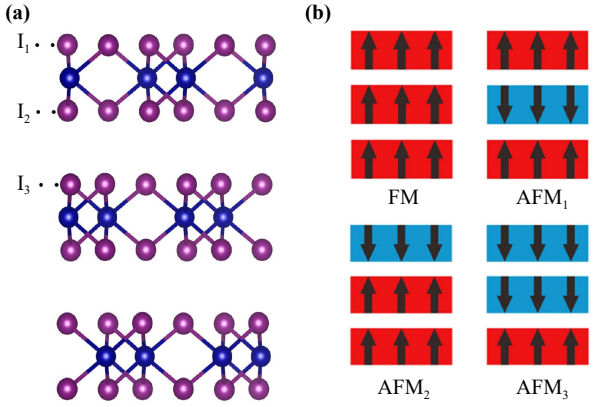

Fig. 5 **(a)** Side view of crystal structure of trilayer CrI_3 with one As substitution at three sites I_1, I_2, and I_3. **(b)** Schematic illustration of ferromagnetic and three antiferromagnetic states in trilayer CrI_3.

interlayer ferromagnetic coupling is more stable than the other three states with interlayer antiferromagnetic coupling, which agrees well with the experimental obser-

vation [1]. One can find that the total energy of As substitution at I_3 site is the lowest, indicating the most stable structure. Therefore, we show that the strong interlayer ferromagnetic coupling can also be established in trilayer CrI_3 via As doping.

5 Conclusion

In summary, we demonstrate that the interlayer ferromagnetic coupling can be realized in both bilayer and trilayer CrI_3 by doping nonmagnetic elements. Our finding provides a new evidence that the interlayer ferromagnetic coupling in CrI_3 thin films may be related to the formation of localized spin-polarized state, and also provides an alternative scheme for the realization of CrI_3 based ferromagnetic semiconductor.

Declarations The authors declare that they have no competing interests and there are no conflicts.

Acknowledgements This work was financially supported by the National Natural Science Foundation of China (Nos. 11974098 and 11974327), the Natural Science Foundation of Hebei Province (No. A2023205017), the Science Foundation of Hebei Normal University (No. 2019B16), the Fundamental Research Funds for the Central Universities (Nos. WK2030020032 and WK2340000082), and Anhui Initiative in Quantum Information Technologies. The supercomputing services of AM-HPC and USTC are gratefully acknowledged.

References

1. B. Huang, G. Clark, E. Navarro-Moratalla, D. R. Klein, R. Cheng, K. L. Seyler, D. Zhong, E. Schmidgall, M. A. McGuire, D. H. Cobden, W. Yao, D. Xiao, P. Jarillo-Herrero, and X. Xu, Layer-dependent ferromagnetism in a van der Waals crystal down to the monolayer limit, *Nature* 546(7657), 270 (2017)
2. C. Gong, L. Li, Z. Li, H. Ji, A. Stern, Y. Xia, T. Cao, W. Bao, C. Wang, Y. Wang, Z. Q. Qiu, R. J. Cava, S. G. Louie, J. Xia, and X. Zhang, Discovery of intrinsic ferromagnetism in two-dimensional van der Waals crystals, *Nature* 546(7657), 265 (2017)
3. Y. Deng, Y. Yu, Y. Song, J. Zhang, N. Z. Wang, Z. Sun, Y. Yi, Y. Z. Wu, S. Wu, J. Zhu, J. Wang, X. H. Chen, and Y. Zhang, Gate-tunable room-temperature ferromagnetism in two-dimensional Fe_3GeTe_2, *Nature* 563(7729), 94 (2018)
4. M. Gibertini, M. Koperski, A. F. Morpurgo, and K. S. Novoselov, Magnetic 2D materials and heterostructures, *Nat. Nanotechnol.* 14(5), 408 (2019)
5. D. Zhong, K. L. Seyler, X. Linpeng, R. Cheng, N. Sivadas, B. Huang, E. Schmidgall, T. Taniguchi, K. Watanabe, M. A. McGuire, W. Yao, D. Xiao, K. M. C. Fu, and X. Xu, Van der Waals engineering of ferromagnetic semiconductor heterostructures for spin and valleytronics, *Sci. Adv.* 3(5), e1603113 (2017)
6. K. L. Seyler, D. Zhong, B. Huang, X. Linpeng, N. P. Wilson, T. Taniguchi, K. Watanabe, W. Yao, D. Xiao, M. A. McGuire, K. M. C. Fu, and X. Xu, Valley manipulation by optically tuning the magnetic proximity effect in WSe_2/CrI_3 heterostructures, *Nano Lett.* 18(6), 3823 (2018)
7. K. Zollner, M. Gmitra, and J. Fabian, Electrically tunable exchange splitting in bilayer graphene on monolayer $Cr_2X_2Te_6$ with X = Ge, Si, and Sn, *New J. Phys.* 20(7), 073007 (2018)
8. T. Song, X. Cai, M. W. Y. Tu, X. Zhang, B. Huang, N. P. Wilson, K. L. Seyler, L. Zhu, T. Taniguchi, K. Watanabe, M. A. McGuire, D. H. Cobden, D. Xiao, W. Yao, and X. Xu, Giant tunneling magnetoresistance in spin-filter van der Waals heterostructures, *Science* 360(6394), 1214 (2018)
9. D. R. Klein, D. MacNeill, J. L. Lado, D. Soriano, E. Navarro-Moratalla, K. Watanabe, T. Taniguchi, S. Manni, P. Canfield, J. Fernández-Rossier, and P. Jarillo-Herrero, Probing magnetism in 2D van der Waals crystalline insulators via electron tunneling, *Science* 360(6394), 1218 (2018)
10. C. Cardoso, D. Soriano, N. A. García-Martínez, and J. Fernández-Rossier, Van der Waals spin valves, *Phys. Rev. Lett.* 121(6), 067701 (2018)
11. Z. Wang, I. Gutiérrez-Lezama, N. Ubrig, M. Kroner, M. Gibertini, T. Taniguchi, K. Watanabe, A. Imamoğlu, E. Giannini, and A. F. Morpurgo, Very large tunneling magnetoresistance in layered magnetic semiconductor CrI_3, *Nat. Commun.* 9(1), 2516 (2018)
12. D. Ghazaryan, M. T. Greenaway, Z. Wang, V. H. Guarochico-Moreira, I. J. Vera-Marun, J. Yin, Y. Liao, S. V. Morozov, O. Kristanovski, A. I. Lichtenstein, M. I. Katsnelson, F. Withers, A. Mishchenko, L. Eaves, A. K. Geim, K. S. Novoselov, and A. Misra, Magnon-assisted tunnelling in van der Waals heterostructures based on $CrBr_3$, *Nat. Electron.* 1(6), 344 (2018)
13. B. Huang, G. Clark, D. R. Klein, D. MacNeill, E. Navarro-Moratalla, K. L. Seyler, N. Wilson, M. A. McGuire, D. H. Cobden, D. Xiao, W. Yao, P. Jarillo-Herrero, and X. Xu, Electrical control of 2D magnetism in bilayer CrI_3, *Nat. Nanotechnol.* 13(7), 544 (2018)
14. Z. Wang, M. Gibertini, D. Dumcenco, T. Taniguchi, K. Watanabe, E. Giannini, and A. F. Morpurgo, Determining the phase diagram of atomically thin layered antiferromagnet $CrCl_3$, *Nat. Nanotechnol.* 14(12), 1116 (2019)
15. Y. Wang, F. Zhang, M. Zeng, H. Sun, Z. Hao, Y. Cai, H. Rong, C. Zhang, C. Liu, X. Ma, L. Wang, S. Guo, J. Lin, Q. Liu, C. Liu, and C. Chen, Intrinsic magnetic topological materials, *Front. Phys.* 18(2), 21304 (2023)
16. M. Kim, P. Kumaravadivel, J. Birkbeck, W. Kuang, S. G. Xu, D. G. Hopkinson, J. Knolle, P. A. McClarty, A. I. Berdyugin, M. Ben Shalom, R. V. Gorbachev, S. J. Haigh, S. Liu, J. H. Edgar, K. S. Novoselov, I. V. Grigorieva, and A. K. Geim, Micromagnetometry of two-dimensional ferromagnets, *Nat. Electron.* 2(10), 457 (2019)
17. B. Karpiak, A. W. Cummings, K. Zollner, M. Vila, D. Khokhriakov, A. M. Hoque, A. Dankert, P. Svedlindh, J. Fabian, S. Roche, and S. P. Dash, Magnetic proximity in a van der Waals heterostructure of magnetic insulator and graphene, *2D Mater.* 7(1), 015026 (2019)

18. N. Sivadas, S. Okamoto, X. Xu, C. J. Fennie, and D. Xiao, Stacking-dependent magnetism in bilayer CrI_3, *Nano Lett.* 18(12), 7658 (2018)
19. D. Wang and B. Sanyal, Systematic study of monolayer to trilayer CrI_3: Stacking sequence dependence of electronic structure and magnetism, *J. Phys. Chem. C* 125(33), 18467 (2021)
20. P. Jiang, C. Wang, D. Chen, Z. Zhong, Z. Yuan, Z. Y. Lu, and W. Ji, Stacking tunable interlayer magnetism in bilayer CrI_3, *Phys. Rev. B* 99(14), 144401 (2019)
21. S. W. Jang, M. Y. Jeong, H. Yoon, S. Ryee, and M. J. Han, Microscopic understanding of magnetic interactions in bilayer CrI_3, *Phys. Rev. Mater.* 3(3), 031001 (2019)
22. D. Soriano, C. Cardoso, and J. Fernández-Rossier, Interplay between interlayer exchange and stacking in CrI_3 bilayers, *Solid State Commun.* 299, 113662 (2019)
23. L. Thiel, Z. Wang, M. A. Tschudin, D. Rohner, I. Gutiérrez-Lezama, N. Ubrig, M. Gibertini, E. Giannini, A. F. Morpurgo, and P. Maletinsky, Probing magnetism in 2D materials at the nanoscale with single-spin microscopy, *Science* 364(6444), 973 (2019)
24. N. Ubrig, Z. Wang, J. Teyssier, T. Taniguchi, K. Watanabe, E. Giannini, A. F. Morpurgo, and M. Gibertini, Low-temperature monoclinic layer stacking in atomically thin CrI_3 crystals, *2D Mater.* 7(1), 015007 (2020)
25. H. H. Kim, B. Yang, T. Patel, F. Sfigakis, C. Li, S. Tian, H. L. Lei, and A. W. Tsen, One million percent tunnel magnetoresistance in a magnetic van der Waals heterostructure, *Nano Lett.* 18(8), 4885 (2018)
26. M. A. McGuire, H. Dixit, V. R. Cooper, and B. C. Sales, Coupling of crystal structure and magnetism in the layered, ferromagnetic insulator CrI_3, *Chem. Mater.* 27(2), 612 (2015)
27. S. Jiang, L. Li, Z. Wang, K. F. Mak, and J. Shan, Controlling magnetism in 2D CrI_3 by electrostatic doping, *Nat. Nanotechnol.* 13(7), 549 (2018)
28. C. Xu, Q. J. Wang, B. Xu, and J. Hu, Effect of biaxial strain and hydrostatic pressure on the magnetic properties of bilayer CrI_3, *Front. Phys.* 16(5), 53502 (2021)
29. R. Xu and X. Zou, Electric field-modulated magnetic phase transition in van der Waals CrI_3 bilayers, *J. Phys. Chem. Lett.* 11(8), 3152 (2020)
30. D. Soriano and M. I. Katsnelson, Magnetic polaron and antiferromagnetic-ferromagnetic transition in doped bilayer CrI_3, *Phys. Rev. B* 101(4), 041402(R) (2020)
31. P. E. Blöchl, Projector augmented-wave method, *Phys. Rev. B* 50(24), 17953 (1994)
32. G. Kresse and J. Furthmuller, Efficient iterative schemes for *ab initio* total-energy calculations using a plane-wave basis set, *Phys. Rev. B* 54(16), 11169 (1996)
33. G. Kresse and D. Joubert, From ultrasoft pseudopotentials to the projector augmented-wave method, *Phys. Rev. B* 59(3), 1758 (1999)
34. J. P. Perdew, K. Burke, and M. Ernzerhof, Generalized gradient approximation made simple, *Phys. Rev. Lett.* 77(18), 3865 (1996)
35. S. Grimme, Semiempirical GGA-type density functional constructed with a long-range dispersion correction, *J. Comput. Chem.* 27(15), 1787 (2006)
36. V. I. Anisimov, J. Zaanen, and O. K. Andersen, Band theory and Mott insulators: Hubbard U instead of Stoner I, *Phys. Rev. B* 44(3), 943 (1991)
37. S. L. Dudarev, G. A. Botton, S. Y. Savrasov, C. J. Humphreys, and A. P. Sutton, Electron-energy-loss spectra and the structural stability of nickel oxide: An LSDA+U study, *Phys. Rev. B* 57(3), 1505 (1998)
38. M. Yang, H. Shu, P. Tang, P. Liang, D. Cao, and X. Chen, Intrinsic polarization-induced enhanced ferromagnetism and self-doped p–n junctions in $CrBr_3$/GaN van der Waals heterostructures, *ACS Appl. Mater. Interfaces* 13(7), 8764 (2021)
39. C. Franchini, M. Reticcioli, M. Setvin, and U. Diebold, Polarons in materials, *Nat. Rev. Mater.* 6(7), 560 (2021)
40. J. Heyd, G. E. Scuseria, and M. Ernzerhof, Hybrid functionals based on a screened Coulomb potential, *J. Chem. Phys.* 118(18), 8207 (2003)
41. J. M. Zhang, W. G. Zhu, Y. Zhang, D. Xiao, and Y. G. Yao, Tailoring magnetic doping in the topological insulator Bi_2Se_3, *Phys. Rev. Lett.* 109(26), 266405 (2012)
42. S. Qi, R. Gao, M. Chang, T. Hou, Y. Han, and Z. Qiao, Nonmagnetic doping induced quantum anomalous Hall effect in topological insulators, *Phys. Rev. B* 102(8), 085419 (2020)
43. Y. Han, S. Sun, S. Qi, X. Xu, and Z. Qiao, Interlayer ferromagnetism and high-temperature quantum anomalous Hall effect in p-doped $MnBi_2Te_4$ multilayers, *Phys. Rev. B* 103(24), 245403 (2021)
44. H. Pan, J. B. Yi, L. Shen, R. Q. Wu, J. H. Yang, J. Y. Lin, Y. P. Feng, J. Ding, L. H. Van, and J. H. Yin, Room-temperature ferromagnetism in carbon-doped ZnO, *Phys. Rev. Lett.* 99(12), 127201 (2007)
45. S. Grimme, J. Antony, S. Ehrlich, and S. Krieg, A consistent and accurate ab initio parametrization of density functional dispersion correction (DFT-D) for the 94 elements H-Pu, *J. Chem. Phys.* 132(15), 154104 (2010)
46. M. Dion, H. Rydberg, E. Schröder, D. C. Langreth, and B. I. Lundqvist, Van der Waals density functional for general geometries, *Phys. Rev. Lett.* 92(24), 246401 (2004)
47. K. Lee, E. D. Murray, L. Kong, B. I. Lundqvist, and D. C. Langreth, Higher-accuracy van der Waals density functional, *Phys. Rev. B* 82(8), 081101(R) (2010)
48. J. Klimeš, D. R. Bowler, and A. Michaelides, Van der Waals density functionals applied to solids, *Phys. Rev. B* 83(19), 195131 (2011)
49. J. Klimeš, D. R. Bowler, and A. Michaelides, Chemical accuracy for the van der Waals density functional, *J. Phys.: Condens. Matter* 22(2), 022201 (2010)
50. T. Li, S. Jiang, N. Sivadas, Z. Wang, Y. Xu, D. Weber, J. E. Goldberger, K. Watanabe, T. Taniguchi, C. J. Fennie, K. Fai Mak, and J. Shan, Pressure-controlled interlayer magnetism in atomically thin CrI_3, *Nat. Mater.* 18(12), 1303 (2019)
51. T. Song, Z. Fei, M. Yankowitz, Z. Lin, Q. Jiang, K. Hwangbo, Q. Zhang, B. Sun, T. Taniguchi, K. Watanabe, M. A. McGuire, D. Graf, T. Cao, J. H. Chu, D. H. Cobden, C. R. Dean, D. Xiao, and X. Xu, Switching 2D magnetic states via pressure tuning of layer stacking, *Nat. Mater.* 18(12), 1298 (2019)
52. J. Xia, J. Yan, Z. Wang, Y. He, Y. Gong, W. Chen, T.

C. Sum, Z. Liu, P. M. Ajayan, and Z. Shen, Strong coupling and pressure engineering in WSe_2–$MoSe_2$ heterobilayers, *Nat. Phys.* 17(1), 92 (2021)

53. W. Zhu, C. Song, Y. Zhou, Q. Wang, H. Bai, and F. Pan, Insight into interlayer magnetic coupling in 1T-type transition metal dichalcogenides based on the stacking of nonmagnetic atoms, *Phys. Rev. B* 103(22), 224404 (2021)
54. J. W. Xiao and B. H. Yan, An electron-counting rule to determine the interlayer magnetic coupling of the van der Waals materials, *2D Mater.* 7(4), 045010 (2020)
55. Z. Li, J. Li, K. He, X. Wan, W. Duan, and Y. Xu, Tunable interlayer magnetism and band topology in van der Waals heterostructures of $MnBi_2Te_4$-family materials, *Phys. Rev. B* 102(8), 081107(R) (2020)
56. W. Zhu, C. Song, L. Liao, Z. Zhou, H. Bai, Y. Zhou, and F. Pan, Quantum anomalous Hall insulator state in ferromagnetically ordered $MnBi_2Te_4/VBi_2Te_4$ heterostructures, *Phys. Rev. B* 102(8), 085111 (2020)
57. N. Liu, S. Zhou, and J. Zhao, High-Curie-temperature ferromagnetism in bilayer CrI_3 on bulk semiconducting substrates, *Phys. Rev. Mater.* 4(9), 094003 (2020)
58. J. M. D. Coey, M. Venkatesan, and C. B. Fitzgerald, Donor impurity band exchange in dilute ferromagnetic oxides, *Nat. Mater.* 4(2), 173 (2005)
59. E. J. Telford, A. H. Dismukes, R. L. Dudley, R. A. Wiscons, K. Lee, D. G. Chica, M. E. Ziebel, M. G. Han, J. Yu, S. Shabani, A. Scheie, K. Watanabe, T. Taniguchi, D. Xiao, Y. Zhu, A. N. Pasupathy, C. Nuckolls, X. Zhu, C. R. Dean, and X. Roy, Coupling between magnetic order and charge transport in a two-dimensional magnetic semiconductor, *Nat. Mater.* 21(7), 754 (2022)